International Journal of Bifurcation and Chaos, Vol. 11, No. 11 (2001) 2817–2822

SPATIOTEMPORAL STRUCTURES IN UNDOPED PHOTOEXCITED SEMICONDUCTOR SUPERLATTICES

A. PERALES and L. L. BONILLA
Universidad Carlos III de Madrid, Butarque 15, Leganés 28911, Spain

M. MOSCOSO
Department of Mathematics,
Stanford University, Stanford, CA 94305, USA

J. GALÁN
Departamento de Matemática Aplicada II, Universidad de Sevilla,
Camino de los Descubrimientos, Sevilla 41092, Spain

Received October 2, 2000; Revised January 8, 2001

Semiconductor superlattices are a very interesting example of a nonlinear dynamical system with a large number of degrees of freedom. They show a strongly nonlinear behavior and they are well suited for the observation of current instabilities. In the present work, the dynamical behavior of undoped photoexcited superlattices has been analyzed by numerical continuation methods and bifurcation theory within the framework of a simple drift-diffusion model. The control parameters are the applied dc voltage and the carrier density, which are related to the laser power. We compile our results in a phase diagram and locate the lines where the system undergoes qualitative changes of behavior. The oscillatory regions are related to the appearance and disappearance of Hopf tongue crossings, for which oscillations appear as sub- or supercritical bifurcations. This implies the existence of voltage windows of current oscillations and hysteresis in appropriate parameter ranges, which agrees with recent experimental observations.

1. Introduction

The term *superlattice* was proposed by Esaki and Chang [1974] to refer to a periodic array of quantum wells and barriers. They are grown by alternating a few monolayers of, for example, GaAs (the quantum wells) and AlAs (the barriers) on top of a common substrate. During the growing process the superlattice can be *doped* to produce extra electrons, i.e. to change the carrier density. In this case, the amount of extra electrons cannot be changed once the growing process has been completed. Another way to provide extra electrons to the superlattice is by means of laser illumination. Then, we talk about an *undoped photoexcited* superlattice. The main difference is that the carrier density can be changed externally by varying the power of the laser illumination.

The schematic experimental setup is depicted in Fig. 1; a semiconductor superlattice is placed between a p–n junction, connected to a DC voltage bias (Φ) and illuminated by an external laser (γ) while the time resolved current ($I(t)$) across the circuit is being measured.

Depending on the number and composition of the quantum wells, the carrier density and the applied voltage, a device such as the one described above may produce *stable* electric-field domain solutions [Bonilla *et al.*, 1994], time-dependent oscillations [Kastrup *et al.*, 1997], and, for high

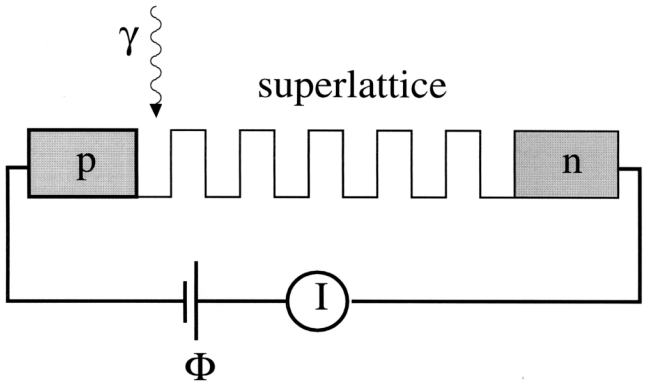

Fig. 1. Schematic experimental setup of a photoexcited superlattice.

temperatures, even undriven chaotic current oscillations [Zhang *et al.*, 1997]. We refer to the book by Grahn [1995] for a comprehensive review of the experiments and the articles by Bonilla *et al.* [1994] and references therein for the theoretical aspects.

In this paper, only undoped photoexcited superlattices have been considered. We investigate the effect of the carrier density (proportional to the square root of the laser power illumination) on the static and dynamical properties of the system. The analysis is done in the framework of a simple drift diffusion model proposed by Bonilla *et al.* [1994].

2. Model

We consider a set of N weakly interacting quantum wells characterized by average values of the electric field E_j, and the carrier densities n_j and p_j (electrons and holes, respectively), where $j = 1, \ldots, N$ denotes the well index. This mean-field-like approach is justified due to the different time scales involved in the transport process. For high enough voltage bias, the scattering time within the quantum wells is much shorter than the tunneling time between adjacent quantum wells. Then, the electric carriers reach a situation of local equilibrium between two consecutive tunneling processes.

We also assume that the lateral extension of the wells and barriers is much larger than the total length of the superlattice. The one-dimensional equations governing the dynamics of the system are: Ampère's equation for the balance of current density I (hole current is neglected), a rate equation for the holes, the Poisson equation averaged over one superlattice period, and the voltage bias condition. The equations are the following

$$\epsilon \frac{dE_j}{dt} + e\, v(E_j) n_j = I \tag{1}$$

$$\frac{dp_j}{dt} = \gamma - r\, n_j\, p_j \tag{2}$$

$$E_j - E_{j-1} = \frac{el}{\epsilon}(n_j - p_j) \tag{3}$$

$$l \sum_{j=1}^{N} E_j = \Phi\,. \tag{4}$$

In these equations, e, l, r and ϵ are the electron charge, the superlattice period, the electron-hole recombination rate and the effective dielectric constant, respectively. The external parameters γ and Φ represent the photogeneration rate, which is proportional to the laser power, and the external voltage, respectively. The effective electron velocity $v(E)$ (proportional to the tunneling probability) exhibits maxima at the resonant fields for which the adjacent levels of neighboring wells are aligned. In the inset of Fig. 2 we plot the function $v(E)$ used in the present work. Those resonances are purely quantum mechanical phenomena that have to be included necessarily in our, otherwise, semiclassical model.

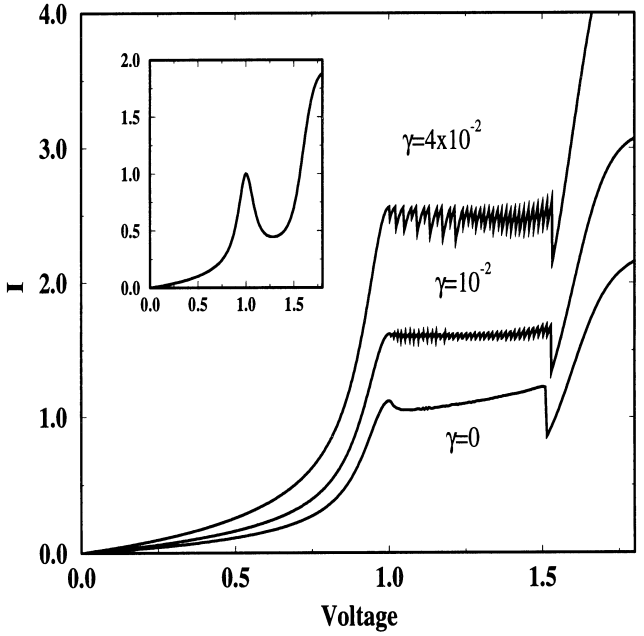

Fig. 2. Intensity voltage bifurcation diagram for a superlattice with $N = 40$ for three different values of the power of the laser.

Equations (1)–(4) have to be solved with appropriated initial conditions plus a boundary condition. The boundary condition $\epsilon(E_1 - E_0)/(el) = \delta$ represents a small charge accumulation in the first quantum well due to the doping of the contact layer before the first barrier.

The results presented below are in dimensionless units by adopting $E_{1-2} = \Delta\varepsilon_{12}/(el)$ as the unit of field, with ε_{12} being the energy separation between the first and the second electron subbands [the maximum of $v(E)$]. This yields a characteristic charge density $n_0 = \epsilon E_{1-2}/(el)$. Finally, for I, γ and Φ the units are $en_0v(E_{1-2})$, rn_0^2 and $E_{1-2}Nl$, respectively.

3. Results

3.1. *Bifurcation diagram*

In this section we study the stationary and the time periodic solutions of our model. The stationary solutions can be calculated taking advantage of the recursive structure of the equations. This results in the discrete mapping

$$E_{j-1} = f(E_j;\, \gamma,\, I) \qquad j = 2, \ldots,\, N \tag{5}$$

with

$$f(E;\, \gamma,\, I) \equiv E - \frac{I}{v(E)} + \frac{\gamma}{I} v(E)\,. \tag{6}$$

The boundary condition implies the relation $I = (\delta + \sqrt{\delta^2 + 4\gamma})v(E_1)/2$ between I and E_1. To solve the stationary problem we fix I (or equivalently E_1), we find the profile $\{E_i\}$, $i = 1, 2, \ldots, N$, by forward iterating the map (5), and calculate the corresponding value of Φ by Eq. (4). Note that I is a good scalar measure of the solution of the system, and therefore the $I - \Phi$ curve corresponds to a stationary bifurcation diagram. In Fig. 2 we plot the current voltage characteristics for $\delta = 10^{-3}$, $N = 40$ and three different values of γ.

A linear stability analysis reveals that for certain values of Φ and γ, multistability and hysteresis are present. We find three different qualitative regimes.

- For small values of γ we have only stable uniform solutions.
- For large values of γ we have multistability and domain solutions.
- For intermediate values of γ and appropriate values of Φ we find self-sustained oscillations.

In Fig. 3(a) we plot the maximum value of the current in arbitrary units as a function of the voltage for $\gamma = 0.02$. The maximum of the current is obtained by direct numerical simulation of Eqs. (1)–(4). We see that the system exhibits oscillatory behavior in a broad range of voltage values and that there are narrow windows with the absence

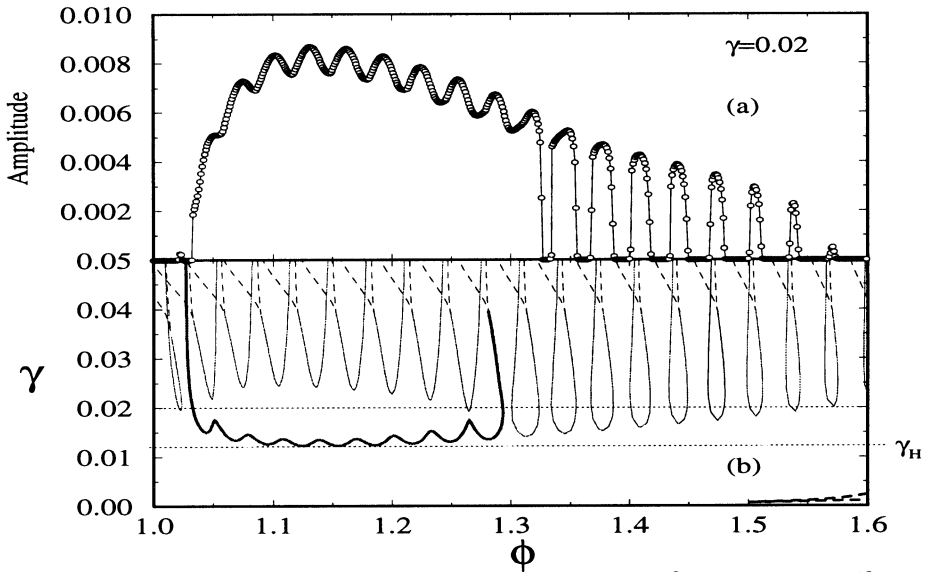

Fig. 3. (a) Amplitude of the current self-oscillations for $\gamma = 0.02$. The windows of oscillations and the subcritical bifurcation are clearly visible. (b) Partial phase diagram for $N = 40$, $c = 10^{-4}$. The solid lines are curves of Hopf points and the dashed are curves of stationary saddle-nodes.

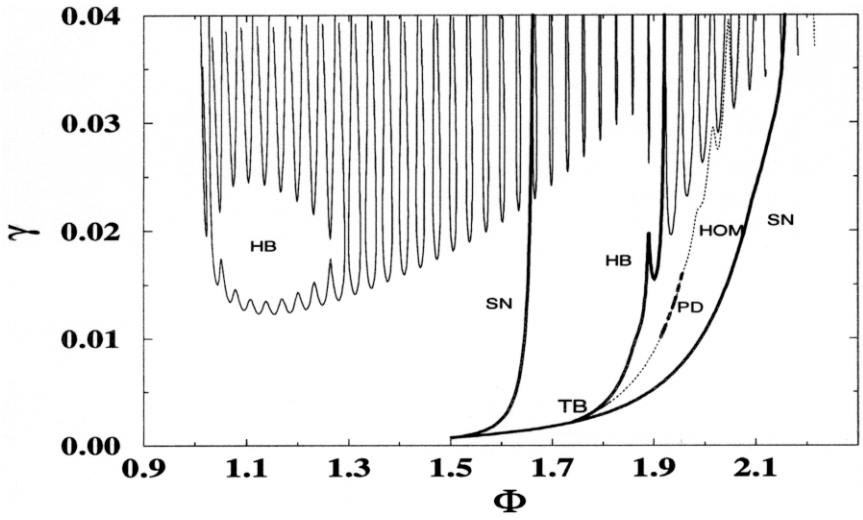

Fig. 4. Total phase diagram. SN stands for Hopf bifurcation, SN for saddle node bifurcation, TB for Takens–Bogdanov bifurcation, PD for period-doubling bifurcation and HOM for homoclinic orbits.

of oscillations. The electric fields at all the quantum wells evolve in a coherent way and depending on the boundary condition, several spatiotemporal structures are possible. See [Carpio *et al.*, 2000] for details.

3.2. *Phase diagram*

In Fig. 3(b) we show the $\gamma - \Phi$ bifurcation set for $1 \leq \Phi \leq 1.6$. The solid thick line is the main Hopf curve, the solid thin lines are secondary Hopf curves, and the dashed lines correspond to curves of saddle-node of stationary solutions. According to this figure, there is a minimum value γ_H of the parameter γ, below which there is only one stationary solution for each value of Φ. For $\gamma > \gamma_H$ fixed, the stationary solution loses its stability at a critical value of Φ via a Hopf bifurcation. Then, a branch of time periodic solutions appears. By fixing a convenient value of γ, for instance $\gamma = 0.02$, we observe the existence of regions (*windows*) where time-periodic solutions appear, followed by regions where there are no oscillations. This agrees with recent experimental observations by Ohtani *et al.* [1999]. We note that the Hopf bifurcations are either *supercritical* or *subcritical* depending on the value of γ. For higher values of γ we find curves of saddle-node of stationary solutions corresponding to the region of electric-field domain solutions.

In Fig. 4 we show the total $\gamma - \Phi$ phase diagram of the system with all the curves, except the curves of saddle-nodes in Fig. 3(b). Besides the Hopf curves (solid thin lines) already shown in Fig. 3(b), we observe a curve of saddle-nodes of stationary solutions (solid thick line) and a curve of homoclinic orbits (dotted line). These three curves are born at a Takens–Bogdanov bifurcation point (TB). We have paid special attention to the curve of homoclinic orbits. Away from the TB point, the saddle could evolve to a saddle-focus, develop spatial structure, and become a Šil'nikov homoclinic orbit. In this case, we expect a rich variety of periodic and aperiodic motions in its neighborhood. We have found period-doubling bifurcations for large values of Φ (dashed lines in Fig. 4) and this may be a hint of a richer dynamical behavior. This point is a significant difference with the doped case reported by Moscoso *et al.* [2000]. However, *we have not found any signature of time-chaotic solutions.*

3.3. *Dependence of the frequency on the parameter γ*

In Fig. 5 we have plotted the frequency spectra of the current self-oscillations versus the applied bias voltage. The existence of voltage windows of current oscillations is clearly visible. Furthermore, multistability of periodic solutions is possible in an appropriate range of parameters. An analysis of the dependence of the oscillation frequency on the carrier density, which may have important consequences for the applications, gives the following scenarios.

(i) The oscillation frequency decreases with increasing carrier density until the oscillation

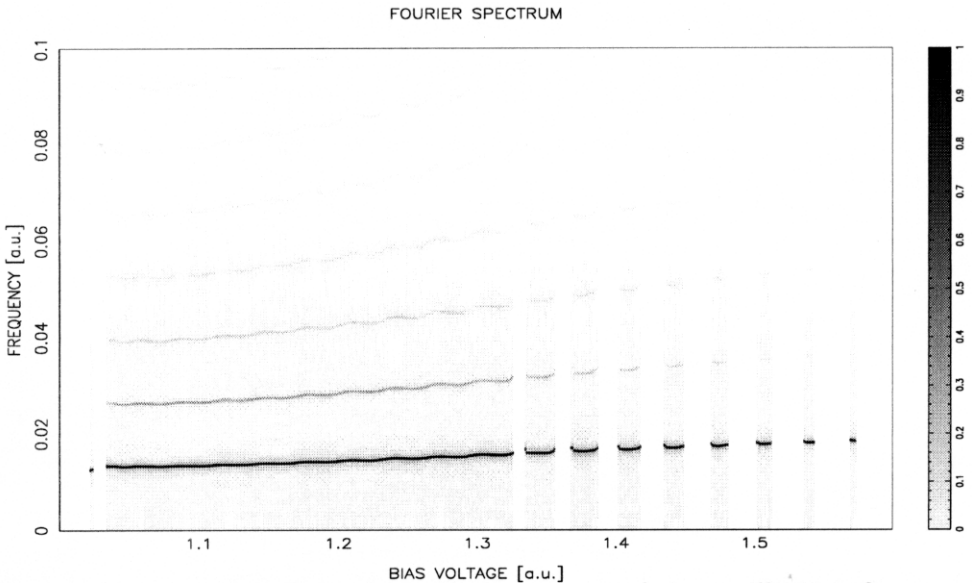

Fig. 5. Contour plot of the frequency spectrum of the oscillations for $\gamma = 0.02$ as a function of the applied voltage. The presence of higher harmonics reflects the nonlinear character of the oscillations.

amplitude shrinks to zero at large carrier densities (supercritical Hopf bifurcation).

(ii) The same behavior as in case (i), but the amplitude remains almost constant even at large carrier densities, for which the oscillations disappear (subcritical Hopf bifurcation). In this case, hysteresis can be observed in the time-averaged I–V characteristics. By sweeping up the carrier density, the current exhibits a jump at a certain value, while the jump occurs at a smaller carrier density, when the sweep direction is reversed.

(iii) Before the oscillations disappear, the frequency decreases abruptly with increasing carrier density (homoclinic connection). The amplitude of the oscillation remains almost constant, but no hysteresis can be observed.

4. Conclusions

In this work we have studied in detail the bifurcation behavior of a drift model for an undoped semiconductor superlattice. Our results can be used for a better understanding of the experimental data. In fact, the information contained in the bifurcation set (Fig. 4) can be used to design new samples and predict bifurcation scenarios. We have shown that qualitatively different behavior can be reached depending on the values of Φ and γ, which are proportional to the external DC voltage applied and the doping density in the quantum wells. The possibility of building a tunable room temperature GHz oscillator is of particular technological interest.

The interplay between Hopf, homoclinic and saddle-node bifurcations gives rise to a rich phase diagram whose details have been thoroughly investigated. The presence of domain solutions is crucial for the disappearance of the oscillatory behavior. The organizing centers for the long time dynamics in a broad range of parameters are multiple Takens–Bogdanov bifurcation points and degenerate Hopf bifurcation points.

In conclusion, we have obtained a complete understanding of the dynamics of the model and we have predicted new interesting dynamical phenomena that could be relevant for the design of new semiconductor devices. The presence of homoclinic bifurcations and the possibility of temporal chaotic solutions are still under study.

Acknowledgments

We thank R. Merlin, H. T. Grahn, M. Kindelan, A. Wacker, E. Freire and A. Rodríguez-Luís for fruitful discussions. This work has been partially supported by Junta de Andalucía and by the DGES grants PB98-0142 and PB1182.

References

Bonilla, L. L., Galán, J., Cuesta, J. A., Martínez, F. & Molera, J. M. [1994] "Dynamics of electric-field

domains and oscillations of the photocurrent in a simple superlattice model," *Phys. Rev.* **B50**, 8644–8657.

Carpio, A., Bonilla, L. L., Wacker, A. & Schöll, E. [2000] "Wave fronts may move upstream in semiconductor superlattices," *Phys. Rev.* **E61**, 4866–4876.

Esaki, L. & Chang, L. L. [1974] "New transport phenomenon in a semiconductor superlattice," *Phys. Rev. Lett.* **33**, 495–498.

Grahn, H. T. [1995] *Semiconductor Superlattices*; *Growth and Electronic Properties* (World Scientific, Singapore).

Kastrup, J., Hey, R., Ploog, K., Grahn, H. T., Bonilla, L. L., Kindelan, M., Moscoso, M., Wacker, A. & Galán, J. [1997] "Electrically tunable GHz oscillations in doped GaAs–AlAs superlattices," *Phys. Rev.* **B55**, 2476–2488.

Moscoso, M., Galán, J. & Bonilla, L. L. [2000] "Bifurcation behavior of a superlattice model," *SIAM J. Appl. Math.* **60**, 2029–2057.

Ohtani, N., Egami, N., Grahn, H. T. & Ploog, K. [1999] "Phase diagram of static and dynamic electric field domain formation in semiconductor superlattices," *Physica* **B272**, 205–208.

Zhang, Y., Klann, R., Ploog, K. H. & Grahn, H. T. [1997] "Synchronization and chaos induced by resonant tunneling in GaAs/AlAs superlattices," *Phys. Rev. Lett.* **77**, 3001–3004.